Monthly Notices
of the
ROYAL ASTRONOMICAL SOCIETY

MNRAS **485,** 4052–4059 (2019)
Advance Access publication 2019 March 8

doi:10.1093/mnras/stz681

The Li–age correlation: the Sun is unusually Li deficient for its age

M. Carlos,[1]★ J. Meléndez,[1] L. Spina,[2] L. A. dos Santos,[3] M. Bedell,[4] I. Ramirez,[5] M. Asplund,[6] J. L. Bean,[7] D. Yong,[6] J. Yana Galarza[1] and A. Alves-Brito[8]

[1]*Departamento de Astronomia, IAG, Universidade de São Paulo, Rua do Matão 1226, São Paulo 05509-900, Brazil*
[2]*Monash Centre for Astrophysics, School of Physics and Astronomy, Monash University, VIC 3800, Australia*
[3]*Observatoire de l'Université de Genéve, 51 chemin des Maillettes, CH-1290 Versoix, Switzerland*
[4]*Center for Computational Astrophysics, Flatiron Institute, 162 5th Avenue, New York, NY 10010, USA*
[5]*Tacoma Community College, 6501 South 19th Street, Tacoma, WA 98466-7400, USA*
[6]*Research School of Astronomy and Astrophysics, The Australian National University, Cotter Road, Canberra, ACT 2611, Australia*
[7]*Department of Astronomy and Astrophysics, 5640 S. Ellis Ave, Chicago, IL 60637, USA*
[8]*Instituto de Física, Universidade Federal do Rio Grande do Sul, Av. Bento Gonçalves 9500, 90040-060 Porto Alegre, RS, Brazil*

Accepted 2019 March 5. Received 2019 February 21; in original form 2019 January 8

ABSTRACT

This work aims to examine in detail the depletion of lithium in solar twins to better constrain stellar evolution models and investigate its possible connection with exoplanets. We employ spectral synthesis in the region of the asymmetric 6707.75 Å Li I line for a sample of 77 stars plus the Sun. As in previous works based on a smaller sample of solar twins, we find a strong correlation between Li depletion and stellar age. In addition, for the first time we show that the Sun has the lowest Li abundance in comparison with solar twins at similar age (4.6 ± 0.5 Gyr). We compare the lithium content with the condensation temperature slope for a subsample of the best solar twins and determine that the most lithium-depleted stars also have fewer refractory elements. We speculate whether the low lithium content in the Sun might be related to the particular configuration of our Solar system.

Key words: techniques: spectroscopic – Sun: abundances – stars: abundances – stars: evolution – planetary systems – stars: solar-type.

1 INTRODUCTION

The importance of lithium in astronomy ranges from cosmological to stellar evolution questions, and could even be related to exoplanets. The *cosmological Li problem* is related to the mismatch between the Li content produced during big bang nucleosynthesis and the one measured in old halo dwarf stars (Spite & Spite 1982); a disagreement of about a factor of four is found (Ryan, Norris & Beers 1999; Asplund et al. 2006; Bonifacio et al. 2007; Matsuno et al. 2017).

In the context of Galactic chemical evolution, Li abundances obtained in thin disc stars indicate a production of this element at this component of the Galaxy, with the production mechanisms still in debate (Ramírez et al. 2012; Bensby & Lind 2018; Cescutti & Molaro 2018; Fu et al. 2018).

Regarding stellar evolution, the Li-rich giant problem is related to how some observed giant stars have higher content of Li despite the expectation that this element is destroyed during their first dredge-up phase due to its fragile nature (Casey et al. (Aguilera-Gómez et al. 2016; Casey et al. 2016), as seen in standard stellar evolution models. The work of Charbonnel & Lagarde (2010) presented a non-standard stellar evolution model considering thermohaline instability and rotation-induced mixing and they were able to reproduce the Li behaviour in red giants. The non-standard stellar nucleosynthesis presented in Yan et al. (2018) might explain the observations of Li-rich giants in a particular short stellar evolution phase. See also recent papers by Deepak & Reddy (2019) and Casey et al. (2019).

Despite many observational and theoretical efforts, the origin of the observed Li depletion in solar-like stars is not well established yet and remains hotly debated in the literature. Albeit likely related to internal depletion during the lifetime of the star, more Li abundances are necessary to better constrain non-standard evolution stellar models that take into consideration different internal motions of stars. The extra mixing is necessary since Li is destroyed through the reaction ^{7}Li(p, α)α at temperatures of $\sim 2.5 \times 10^{6}$ K near the base of the convective envelope in sun-like stars. Those non-standard evolution models can include gravity waves (Charbonnel & Talon 2005), rotation-induced mixing and diffusion (Do Nascimento et al. 2009), rotation-driven turbulent diffusion (Denissenkov 2010), and overshooting and gravitational settling (Xiong & Deng 2009).

Several works in the literature discuss the factors influencing lithium depletion in solar-type stars such as occurrence of planets (Delgado Mena et al. 2014), binarity (Zahn 1994; Beck et al. 2017),

★ E-mail: marilia.carlos@usp.br

stellar age (Carlos, Nissen & Meléndez 2016), or even planet engulfment (Montalbán & Rebolo 2002; Sandquist et al. 2002). Those factors can be as important as the specific parameters of stars, which also influence the amount of lithium burning, such as the convective zone thickness that depends on the mass and metallicity of a star.

According to Takeda et al. (2010) and Gonzalez, Carlson & Tobin (2010), the difference in the stellar angular momentum could cause different amounts of Li burnt. They claim that there is an increase in the amount of Li burning, the lower the angular momentum is, and thus the presence of planets or solar twins in a binary system should present different amounts of lithium in comparison with single field solar twins with the same stellar parameters and age. This is argued by Israelian et al. (2009), Delgado Mena et al. (2014), and Zahn (1994), but it is probably a secondary effect that accounts for only a small fraction of the total depletion (Pavlenko et al. 2018).

As discussed in Beck et al. (2017), Li abundances vary with stellar rotation that depends on stellar age (dos Santos et al. 2016). This is in agreement with various works that indicate that the Li content in solar twins is depleted as the stars age (Baumann et al. 2010; Monroe et al. 2013; Meléndez et al. 2014; Carlos et al. 2016). More recently, Liu et al. (2016) obtained $A(Li)_{NLTE} = 1.36^{+0.08}_{-0.07}$ dex for one solar twin in the open cluster M67, which has a well-determined age ($3.47^{+0.70}_{-0.45}$ Gyr, Gaia Collaboration 2018). The A(Li) found is in agreement with the relation shown in Carlos et al. (2016), based on field solar twins.

In contrast, Thévenin et al. (2017) analysed solar twins with stellar parameters in the same interval as the sample of Carlos et al. (2016), and built a stellar evolution model, concluding that the Li is mainly depleted during the pre-main-sequence phase, and not during all the main sequence as suggested by Carlos et al. (2016). Thus, it is imperative to our understanding of stellar interiors and the mechanisms of Li depletion to increase the solar twins sample in order to perform more detailed comparisons.

Following the study performed by Carlos et al. (2016), in which we analysed a sample of 21 solar twins, we present here the analysis of a broader sample of 77 solar twins plus the Sun. In this larger sample we have more than 10 new solar twins in the 0–2 Gyr age interval in contrast with just only one object at the same interval in the earlier work of Carlos et al. (2016), adding, thus, valuable information on stellar structure evolution at early ages in the main-sequence phase.

The paper is organized as follows: in Section 2, we discuss the sample and the stellar parameters adopted; in Section 3, we describe the analysis; Section 4 shows the results and discussion and the conclusions are presented in Section 5.

2 SAMPLE

The sample is composed of 77 solar twins plus the Sun. The spectra are from the HARPS spectrograph (Mayor et al. 2003) of the 3.6m ESO telescope at La Silla, where the solar spectrum was observed with the reflected light from the asteroid Vesta. These stars have spectra with high resolving power (R = 115 000) and high signal-to-noise ($300 \lesssim S/N \lesssim 1800$).

These stars, classified as solar twins (effective temperature approximately within $T_{eff,\odot} \pm 100$ K, surface gravity approximately within $\log g_\odot \pm 0.1$, and metallicity approximately within $[Fe/H]_\odot \pm 0.1$), were selected from the work of Ramírez, Meléndez & Asplund (2014) and analysed in more detail by dos Santos et al. (2017), Spina et al. (2018), and Bedell et al. (2018).

The stars HIP 19911, HIP 67620, and HIP 103983 were removed from the sample due to contamination by a nearby companion, as discussed in dos Santos et al. (2017).

In particular, Spina et al. (2018) measured the stellar parameters and ages found in this work, using high-precision spectroscopy through a differential analysis (e.g. Bedell et al. 2014). The effective temperature, surface gravity, and [Fe/H] were measured using Fe I and Fe II lines in a differential line-by-line method aimed to achieve an excitation and ionization equilibrium balance. Then, the stellar age and masses were calculated using the stellar parameters with Yonsei–Yale isochrones (Yi et al. 2001; Kim et al. 2002).

In addition, the work of dos Santos et al. (2016) determined the projected rotational velocity ($v \sin i$) and macroturbulence velocity (v_{macro}) of a bigger sample that includes all the objects studied here.

Our sample of solar twins has 17 objects in a binary system (as showed in dos Santos et al. 2017 and references therein) and the following five exoplanet systems: HIP 5301 (Naef et al. 2010), HIP 11915 (Bedell et al. 2015), HIP 15527 (Jones et al. 2006), HIP 68468 (Meléndez et al. 2017), and HIP 116906 (Butler et al. 2006).

3 ANALYSIS

The lithium abundance analysis employed here is similar to that described in Carlos et al. (2016). We applied spectral synthesis analysis in the region of the asymmetric 6707.75 Å Li I line using the 2014 July version of the 1D LTE code MOOG (Sneden 1973) and the Kurucz grid of ATLAS9 model atmospheres (Castelli & Kurucz 2004). As in Carlos et al. (2016), the line list from Meléndez et al. (2012), which includes blends from atomic and molecular (CN and C_2) lines, was employed.

In order to estimate the lithium abundances[1] we adopted the values of T_{eff}, [Fe/H], log g, and microturbulence velocity (ξ) from Spina et al. (2018) with v_{macro} and $v \sin i$ from dos Santos et al. (2016).

Fig. 1 shows the observed spectra in comparison with their respective spectral synthesis for different stars. It is worth noting that ^{7}Li shows several components introducing an asymmetry in the profile, and the presence of ^{6}Li, to a lesser extent, also contribute to this asymmetry. However, we are not considering the contribution of ^{6}Li on our spectral synthesis due to its much lower abundance found in the Sun (Asplund et al. 2009).

To calculate the final lithium abundance errors we considered the uncertainties in the continuum setting, the rms deviation of the observed line profile relative to the synthetic spectra, and the stellar parameters. The typical (median) Li abundance error is $\sigma = 0.036$ dex.

After estimating the LTE lithium abundances, the non-LTE (NLTE) abundances were obtained through the INSPECT data base,[2] based on NLTE calculations by Lind, Asplund & Barklem (2009). The median value of the non-LTE corrections for the whole sample is 0.04 ± 0.01 dex; the small standard deviation from the median value in comparison with the typical abundance error shows that the effect of the NLTE corrections in the differential analysis precision can be considered negligible.

The stellar parameters and lithium abundances are presented in Table 1. We measure Li abundances down to values of about

[1]The lithium abundances are given in the notation $A(Li) = \log(\epsilon_{Li}) = \log(N_{Li}/N_H) + 12$, where N_{Li} and N_H are the number densities of lithium and hydrogen, respectively.
[2]www.inspect-stars.com(version 1.0).

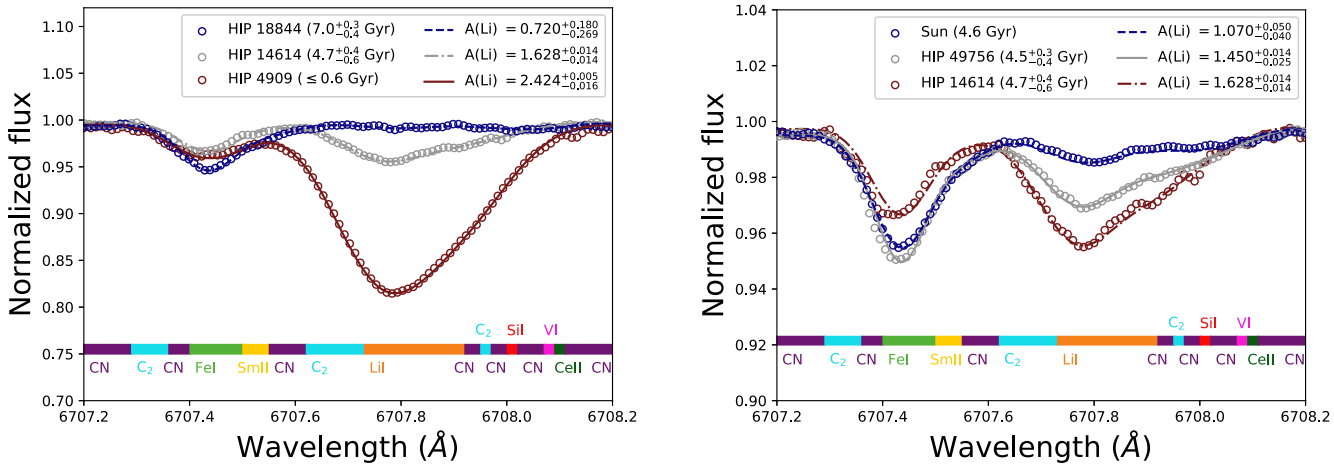

Figure 1. Observed spectra (open circles) in comparison with their respective spectral synthesis for three stars at different ages (left-hand panel) and three stars at similar age (right-hand panel). The bar at the bottom indicates the positions of each atomic or molecular species in the spectra. Notice how younger stars display higher Li abundances (left-hand panel) and how the Sun shows a low Li abundance compared to solar twins of similar age (right-hand panel).

A(Li)∼0.6 dex, and for the high-quality spectra we achieve an upper limit of about A(Li)∼0.3 dex in the most Li-poor solar twins.

4 DISCUSSION

Fig. 2 shows the Li abundances versus stellar age for the whole sample. Non-standard solar models (Charbonnel & Talon 2005; Do Nascimento et al. 2009; Xiong & Deng 2009; Denissenkov 2010; Thévenin et al. 2017), calibrated to fit the Sun, are displayed for comparison. As previously discussed in Carlos et al. (2016), Meléndez et al. (2014), and Monroe et al. (2013), there is a strong correlation between lithium abundances and stellar ages in solar twins (younger stars have more lithium content in comparison with older stars).

In addition, Fig. 2 presents more than 10 new solar twins in the age interval $0.0 \leq$ Age (Gyr) $\lesssim 2.0$, where it is possible to notice the sharp decrease of Li abundances with age. This behaviour might be explained by the fast-rotator nature of young solar-type stars (Pace & Pasquini 2004; Barnes 2007; do Nascimento et al. 2014; dos Santos et al. 2016), which may influence on internal stellar structures (Ballot, Brun & Turck-Chièze 2007; Brown et al. 2008) and enhance internal transport mechanisms (e.g. Schirbel et al. 2015), then affecting how fast Li is burnt in young solar twins. It is interesting to note that at this age interval the data are more well represented by the non-standard evolution solar model of Do Nascimento et al. (2009), which takes in consideration rotation-induced mixing and diffusion. On the other hand, there is no agreement between data and models in the $2.0 \lesssim$ Age (Gyr) $\lesssim 4.0$ interval, where the theoretical predictions anticipate a more significant Li depletion than the shallow Li depletion observed in our sample.

Moreover, the Sun shows a lower lithium abundance in comparison with stars at same age, despite the fact that the work of dos Santos et al. (2016) and Lorenzo-Oliveira et al. (2018) find that the Sun has a typical rotation and activity compared with other solar twins at similar age. Fig. 3 shows the distribution of A(Li) in solar twins at the age interval of $4.1 \leq$ Age (Gyr) ≤ 5.1. The solar Li abundance A(Li)$_\odot = 1.07^{+0.03}_{-0.02}$ dex is the lowest in this age interval, thus confirming that the Sun has the lowest Li abundance when compared to solar twins at similar age. Furthermore, the solar bin lies below 91 per cent of the sample of stars with age 4.6 ± 0.5 Gyr.

In general, the whole sample seems to follow reasonably the A(Li) versus age correlation with a typical scatter of ∼0.2 dex at a given age, estimated from the standard deviation of the Li abundance in 1-Gyr bins (excluding the four outliers HIP 54287, HIP 54582, HIP 64673, and HIP 83276, pointed in Fig. 2). We perform a Spearman correlation test, considering the errors in both axes for the Li-age connection for the whole sample, excluding the outliers mentioned earlier, and find a Spearman rank coefficient $r_s = -0.95$ and a probability of 10^{-37} of our results arising by chance.

To shed some light on these outliers we analyse separately the correlation between A(Li) versus stellar age with [Fe/H], stellar mass and the mass of the convective envelope (Fig. 4), where the mass of the convective envelope was calculated by interpolating the values found in the YaPSI[3] grid of isochrones (Spada et al. 2017).

The upper panel of Fig. 4 shows the dependence between A(Li) and stellar age with [Fe/H] (the typical error is σ([Fe/H]) = 0.004, Spina et al. 2018). We conclude that the sample is homogeneous regarding metallicity and stellar age for this interval; and due to the fact that our sample is composed by only solar twins ($-0.1 \lesssim$[Fe/H]$\lesssim 0.1$), there is no apparent trend in Li abundances with [Fe/H] for a given age. In addition, the outliers HIP 54287, HIP 54582, HIP 64673, and HIP 83276 have substantial differences in [Fe/H] varying from −0.096 dex to 0.107 dex.

In the middle panel of Fig. 4 we present the correlation between A(Li), stellar age, and masses (the typical error is $\sigma(M/M_\odot) = 0.004$, Spina et al. 2018). Likewise the [Fe/H], the stellar mass distribution is somewhat homogeneous in all the age interval, apart from the youngest stars with age $\lesssim$2.0 Gyr where we lack stars with mass $\lesssim 0.98$ M$_\odot$.

The lower panel of Fig. 4 displays A(Li), stellar ages, and masses of the convective envelopes for the whole sample. Following the dependence in mass and [Fe/H] shown in the upper and middle panel of Fig. 4, the sample is somewhat homogeneous for stars with age $\gtrsim$2 Gyr without considering the outliers mentioned earlier.

Discussing specifically the outliers in our sample, three of the four objects (HIP 54582, HIP 64673, and HIP 83276) present a less massive convective envelope; as seen in the lower panel of Fig. 4.

[3]Yale Astro web page: http://www.astro.yale.edu/yapsi/; AIP web page: http://vo.aip.de/yapsi/.

Table 1. Li abundances, ages, masses, and stellar parameters.

Star	A(Li) LTE (dex)	A(Li) NLTE (dex)	Age[a] (Gyr)	Mass[a] ($M_\odot$)	T_{eff}^a (K)	log g^a (dex)	[Fe/H][a] (dex)	Notes
HIP 1954	$1.340^{+0.028}_{-0.061}$	$1.380^{+0.028}_{-0.061}$	$4.80^{+0.30}_{-0.80}$	0.970	5720	4.46	− 0.090	
HIP 3203	$2.450^{+0.005}_{-0.005}$	$2.452^{+0.005}_{-0.005}$	≤0.50	1.038	5868	4.54	− 0.050	
HIP 4909	$2.410^{+0.005}_{-0.016}$	$2.424^{+0.005}_{-0.016}$	≤0.60	1.055	5861	4.50	0.048	
HIP 5301	≤0.910	≤0.952	$7.30^{+0.40}_{-0.50}$	0.960	5723	4.40	− 0.074	Exoplanet detected[b]
HIP 6407	$1.770^{+0.014}_{-0.028}$	$1.800^{+0.014}_{-0.028}$	$1.90^{+0.70}_{-0.70}$	1.004	5775	4.51	− 0.058	Spectroscopic binary[c]
HIP 7585	$1.790^{+0.008}_{-0.011}$	$1.829^{+0.008}_{-0.011}$	$3.50^{+0.30}_{-0.50}$	1.043	5822	4.45	0.083	
HIP 8507	$1.530^{+0.042}_{-0.030}$	$1.570^{+0.042}_{-0.030}$	$4.90^{+0.40}_{-0.50}$	0.961	5717	4.46	− 0.099	
HIP 9349	$2.010^{+0.010}_{-0.011}$	$2.036^{+0.010}_{-0.011}$	$0.60^{+0.40}_{-0.30}$	1.036	5818	4.52	− 0.006	
HIP 10175	$1.690^{+0.014}_{-0.022}$	$1.730^{+0.014}_{-0.022}$	$3.10^{+0.40}_{-0.30}$	0.990	5719	4.49	− 0.028	
HIP 10303	$1.490^{+0.014}_{-0.014}$	$1.540^{+0.014}_{-0.014}$	$5.90^{+0.40}_{-0.40}$	1.011	5712	4.40	0.104	
HIP 11915	$1.570^{+0.010}_{-0.014}$	$1.604^{+0.010}_{-0.014}$	$3.60^{+0.50}_{-0.70}$	0.993	5769	4.48	− 0.067	Exoplanet detected[d]
HIP 14501	≤0.220	≤0.260	$8.80^{+0.30}_{-0.30}$	0.979	5738	4.31	− 0.153	Spectroscopic binary[c]
HIP 14614	$1.600^{+0.014}_{-0.014}$	$1.628^{+0.014}_{-0.014}$	$4.70^{+0.40}_{-0.60}$	0.986	5803	4.45	− 0.109	
HIP 15527	$0.640^{+0.141}_{-0.224}$	$0.676^{+0.141}_{-0.224}$	$7.70^{+0.40}_{-0.30}$	0.986	5779	4.34	− 0.064	Exoplanet detected[e]
HIP 18844	$0.670^{+0.180}_{-0.269}$	$0.720^{+0.180}_{-0.269}$	$7.00^{+0.30}_{-0.40}$	0.997	5734	4.37	0.014	Spectroscopic binary[c]
HIP 22263	$2.370^{+0.005}_{-0.010}$	$2.383^{+0.005}_{-0.010}$	$0.80^{+0.30}_{-0.40}$	1.052	5870	4.54	0.037	
HIP 25670	$1.110^{+0.050}_{-0.050}$	$1.160^{+0.050}_{-0.050}$	$5.10^{+0.30}_{-0.30}$	1.010	5760	4.42	0.054	
HIP 28066	$0.710^{+0.054}_{-0.058}$	$0.745^{+0.054}_{-0.058}$	$8.80^{+0.30}_{-0.30}$	0.989	5742	4.30	− 0.147	
HIP 29432	$1.210^{+0.036}_{-0.022}$	$1.245^{+0.036}_{-0.022}$	$5.20^{+0.40}_{-0.40}$	0.969	5762	4.45	− 0.112	
HIP 30037	$0.740^{+0.141}_{-0.224}$	$0.790^{+0.141}_{-0.224}$	$6.70^{+0.50}_{-0.50}$	0.960	5666	4.42	0.007	Spectroscopic binary[c]
HIP 30158	$0.670^{+0.100}_{-0.197}$	$0.720^{+0.100}_{-0.197}$	$7.90^{+0.30}_{-0.30}$	0.963	5678	4.37	− 0.004	
HIP 30476	≤0.270	≤0.315	$9.00^{+0.30}_{-0.30}$	0.990	5709	4.28	− 0.033	
HIP 30502	$0.950^{+0.099}_{-0.094}$	$0.990^{+0.099}_{-0.094}$	$7.00^{+0.40}_{-0.10}$	0.965	5731	4.40	− 0.057	
HIP 33094	$0.620^{+0.166}_{-0.089}$	$0.678^{+0.166}_{-0.089}$	$8.90^{+0.30}_{-0.30}$	1.064	5629	4.11	0.023	
HIP 34511	$1.730^{+0.005}_{-0.022}$	$1.756^{+0.005}_{-0.022}$	$4.00^{+0.50}_{-0.40}$	0.998	5812	4.45	− 0.091	
HIP 36512	$1.200^{+0.036}_{-0.036}$	$1.236^{+0.036}_{-0.036}$	$5.90^{+0.40}_{-0.50}$	0.957	5744	4.45	− 0.126	
HIP 36515	$2.680^{+0.005}_{-0.005}$	$2.667^{+0.005}_{-0.005}$	$0.50^{+0.30}_{-0.30}$	1.031	5855	4.56	− 0.029	
HIP 38072	$1.620^{+0.054}_{-0.028}$	$1.656^{+0.054}_{-0.028}$	$1.00^{+0.80}_{-0.50}$	1.063	5860	4.51	0.085	
HIP 40133	$1.480^{+0.011}_{-0.021}$	$1.530^{+0.011}_{-0.021}$	$5.40^{+0.30}_{-0.30}$	1.040	5745	4.37	0.116	
HIP 41317	$0.690^{+0.081}_{-0.186}$	$0.733^{+0.081}_{-0.186}$	$7.70^{+0.30}_{-0.30}$	0.960	5706	4.39	− 0.081	
HIP 42333	$2.250^{+0.006}_{-0.006}$	$2.280^{+0.006}_{-0.006}$	$1.00^{+0.70}_{-0.40}$	1.069	5846	4.50	0.132	
HIP 43297	$1.590^{+0.014}_{-0.010}$	$1.640^{+0.014}_{-0.010}$	$1.80^{+0.50}_{-0.40}$	1.014	5705	4.51	0.082	
HIP 44713	$0.590^{+0.141}_{-0.355}$	$0.638^{+0.141}_{-0.355}$	$7.70^{+0.30}_{-0.30}$	1.029	5759	4.28	0.063	
HIP 44935	$0.980^{+0.057}_{-0.090}$	$1.020^{+0.057}_{-0.090}$	$6.60^{+0.30}_{-0.40}$	1.009	5771	4.37	0.038	
HIP 44997	$1.140^{+0.043}_{-0.036}$	$1.184^{+0.043}_{-0.036}$	$6.60^{+0.40}_{-0.40}$	0.970	5728	4.41	− 0.012	
HIP 49756	$1.410^{+0.014}_{-0.025}$	$1.450^{+0.014}_{-0.025}$	$4.50^{+0.30}_{-0.40}$	1.010	5789	4.44	0.023	
HIP 54102	$2.170^{+0.011}_{-0.010}$	$2.191^{+0.011}_{-0.010}$	$0.70^{+0.40}_{-0.40}$	1.047	5845	4.51	0.011	Spectroscopic binary[c]
HIP 54287	$1.860^{+0.007}_{-0.011}$	$1.911^{+0.007}_{-0.011}$	$6.50^{+0.30}_{-0.40}$	1.024	5714	4.34	0.107	
HIP 54582	$1.620^{+0.011}_{-0.022}$	$1.640^{+0.011}_{-0.022}$	$6.90^{+0.30}_{-0.30}$	1.034	5883	4.28	− 0.096	Spectroscopic binary[c]
HIP 62039	$0.760^{+0.067}_{-0.184}$	$0.814^{+0.067}_{-0.184}$	$6.20^{+0.40}_{-0.30}$	1.040	5742	4.34	0.104	Spectroscopic binary[c]
HIP 64150	≤0.440	≤0.490	$6.40^{+0.30}_{-0.30}$	1.010	5747	4.37	0.049	Spectroscopic binary[c]
HIP 64673	$1.780^{+0.010}_{-0.036}$	$1.799^{+0.010}_{-0.036}$	$6.00^{+0.40}_{-0.40}$	1.068	5912	4.29	− 0.017	
HIP 64713	$1.420^{+0.014}_{-0.036}$	$1.454^{+0.014}_{-0.036}$	$5.30^{+0.50}_{-0.60}$	0.989	5788	4.44	− 0.043	
HIP 65708	$0.710^{+0.144}_{-0.089}$	$0.750^{+0.144}_{-0.089}$	$9.00^{+0.30}_{-0.30}$	1.009	5746	4.22	− 0.063	Spectroscopic binary[c]
HIP 68468	$1.460^{+0.014}_{-0.071}$	$1.497^{+0.014}_{-0.071}$	$5.50^{+0.30}_{-0.40}$	1.064	5845	4.33	0.071	Exoplanet detected[f]
HIP 69645	$1.040^{+0.057}_{-0.143}$	$1.080^{+0.057}_{-0.143}$	$5.70^{+0.30}_{-0.90}$	0.986	5751	4.44	− 0.026	
HIP 72043	$1.030^{+0.100}_{-0.076}$	$1.060^{+0.100}_{-0.076}$	$6.20^{+0.40}_{-0.30}$	1.026	5845	4.34	− 0.026	Spectroscopic binary[c]
HIP 73241	≤0.180	≤0.240	$8.90^{+0.30}_{-0.30}$	1.031	5661	4.22	0.092	Spectroscopic binary[c]
HIP 73815	$0.870^{+0.099}_{-0.122}$	$0.910^{+0.099}_{-0.122}$	$7.20^{+0.30}_{-0.30}$	1.011	5790	4.33	0.023	
HIP 74389	$2.060^{+0.005}_{-0.013}$	$2.090^{+0.005}_{-0.013}$	$3.90^{+0.30}_{-0.60}$	1.049	5845	4.44	0.083	

Table 1 – *continued*

Star	*A*(Li) LTE (dex)	*A*(Li) NLTE (dex)	Age[a] (Gyr)	Mass[a] ($M_\odot$)	T_{eff}[a] (K)	log *g*[a] (dex)	[Fe/H][a] (dex)	Notes
HIP 74432	$0.590^{+0.156}_{-0.112}$	$0.640^{+0.156}_{-0.112}$	$8.60^{+0.30}_{-0.30}$	1.056	5679	4.17	0.048	
HIP 76114	$0.910^{+0.064}_{-0.085}$	$0.950^{+0.064}_{-0.085}$	$6.60^{+0.30}_{-0.30}$	0.980	5740	4.41	− 0.024	
HIP 77052	$1.510^{+0.018}_{-0.022}$	$1.564^{+0.018}_{-0.022}$	$4.50^{+1.10}_{-0.40}$	0.985	5687	4.45	0.051	Visual binary[c]
HIP 77883	$0.660^{+0.061}_{-0.114}$	$0.710^{+0.061}_{-0.114}$	$7.60^{+0.30}_{-0.40}$	0.970	5699	4.34	0.017	
HIP 79578	$1.940^{+0.005}_{-0.006}$	$1.970^{+0.005}_{-0.006}$	$2.40^{+0.60}_{-0.40}$	1.031	5810	4.47	0.048	Spectroscopic binary[c]
HIP 79672	$1.570^{+0.011}_{-0.011}$	$1.608^{+0.011}_{-0.011}$	$4.20^{+0.30}_{-0.50}$	1.022	5808	4.44	0.041	
HIP 79715	$1.050^{+0.140}_{-0.085}$	$1.080^{+0.140}_{-0.085}$	$6.20^{+0.30}_{-0.40}$	1.000	5816	4.38	− 0.037	
HIP 81746	$0.590^{+0.242}_{-0.112}$	$0.630^{+0.242}_{-0.112}$	$8.10^{+0.30}_{-0.30}$	0.960	5715	4.37	− 0.091	Spectroscopic binary[c]
HIP 83276	$1.670^{+0.018}_{-0.009}$	$1.690^{+0.018}_{-0.009}$	$7.40^{+0.30}_{-0.30}$	1.033	5886	4.24	− 0.093	Spectroscopic binary[c]
HIP 85042	$0.480^{+0.124}_{-0.040}$	$0.533^{+0.124}_{-0.040}$	$7.80^{+0.30}_{-0.30}$	0.970	5685	4.35	0.030	
HIP 87769	$1.570^{+0.064}_{-0.030}$	$1.610^{+0.064}_{-0.030}$	$5.00^{+0.40}_{-1.00}$	1.039	5828	4.40	0.072	Spectroscopic binary[c]
HIP 89650	$1.380^{+0.024}_{-0.081}$	$1.409^{+0.024}_{-0.081}$	$4.30^{+0.70}_{-0.30}$	1.027	5851	4.42	− 0.015	
HIP 95962	$1.230^{+0.021}_{-0.106}$	$1.269^{+0.021}_{-0.106}$	$6.00^{+0.40}_{-0.30}$	1.010	5805	4.38	0.029	
HIP 96160	$1.720^{+0.007}_{-0.029}$	$1.750^{+0.007}_{-0.029}$	$2.60^{+0.40}_{-0.50}$	1.012	5798	4.48	− 0.036	
HIP 101905	$2.120^{+0.010}_{-0.014}$	$2.145^{+0.010}_{-0.014}$	$1.20^{+0.30}_{-0.30}$	1.080	5906	4.50	0.088	
HIP 102040	$2.160^{+0.010}_{-0.010}$	$2.170^{+0.010}_{-0.010}$	$2.40^{+0.40}_{-0.40}$	1.020	5853	4.48	− 0.079	
HIP 102152	$0.580^{+0.212}_{-0.224}$	$0.630^{+0.212}_{-0.224}$	$8.60^{+0.30}_{-0.40}$	0.978	5718	4.33	− 0.016	
HIP 104045	$1.510^{+0.064}_{-0.030}$	$1.550^{+0.064}_{-0.030}$	$4.10^{+0.90}_{-0.30}$	1.027	5826	4.41	0.051	
HIP 105184	$2.230^{+0.011}_{-0.014}$	$2.247^{+0.011}_{-0.014}$	$0.60^{+0.50}_{-0.30}$	1.050	5843	4.51	0.003	
HIP 108158	$0.560^{+0.194}_{-0.252}$	$0.616^{+0.194}_{-0.252}$	$8.10^{+0.30}_{-0.30}$	1.021	5675	4.29	0.055	
HIP 108468	$1.100^{+0.058}_{-0.122}$	$1.127^{+0.058}_{-0.122}$	$7.00^{+0.30}_{-0.30}$	1.006	5841	4.35	− 0.096	
HIP 109821	$0.670^{+0.136}_{-0.234}$	$0.707^{+0.136}_{-0.234}$	$8.90^{+0.30}_{-0.30}$	0.980	5747	4.31	− 0.108	
HIP 114615	$1.860^{+0.014}_{-0.011}$	$1.886^{+0.014}_{-0.011}$	$0.50^{+1.20}_{-0.30}$	1.027	5819	4.51	− 0.063	
HIP 115577	≤0.160	≤0.210	$8.80^{+0.30}_{-0.30}$	1.019	5694	4.26	0.013	
HIP 116906	$0.740^{+0.191}_{-0.112}$	$0.778^{+0.191}_{-0.112}$	$6.70^{+0.30}_{-0.30}$	1.010	5790	4.37	− 0.005	Exoplanet detected[g]
HIP 117367	$1.420^{+0.028}_{-0.058}$	$1.450^{+0.028}_{-0.058}$	$5.70^{+0.30}_{-0.30}$	1.040	5867	4.35	0.024	
HIP 118115	$0.920^{+0.042}_{-0.081}$	$0.960^{+0.042}_{-0.081}$	$8.00^{+0.30}_{-0.30}$	1.013	5798	4.28	− 0.036	
Sun[a]	$1.030^{+0.030}_{-0.020}$	$1.070^{+0.030}_{-0.020}$	4.6	1.000	5777	4.44	0.000	

Notes.
[a]Data from Spina et al. (2018).
[b]Naef et al. (2010).
[c]dos Santos et al. (2017).
[d]Bedell et al. (2015).
[e]Jones et al. (2006).
[f]Meléndez et al. (2017).
[g]Butler et al. (2006).

This might be an effect of the combination of the lower values of [Fe/H] and higher values of stellar mass in comparison with other objects in the sample. Thus, the small size of the convective envelope implies in less Li burning, which causes the discrepancy in the Li content in these three stars in comparison to the rest of the sample.

Although the star HIP 54287 has a 'regular' convective envelope to burn Li at the same extent as other stars at the same bin of age (excluding the outliers), the high Li content indicates that this object could have experienced a planet engulfment, as described in Montalbán & Rebolo (2002) and Sandquist et al. (2002) and as previously discussed in Carlos et al. (2016). If this is the case, we are observing a short-duration event, because according to Théado & Vauclair (2012), thermohaline mixing should dilute the Li overabundance that we observe in about ∼50 million years, or perhaps thermohaline mixing could be less efficient and the Li enhancement remain for longer times (increasing the probability of observing this type of event).

The data presented in Fig. 5 are for the case when we narrow our criteria of solar twins for our sample and consider only objects with mass in the interval $0.98 \leq M/M_\odot \leq 1.02$, and excluding upper limits in Li abundances. For this subsample, the median value for the masses of the convective envelopes is 0.023 ± 0.003 dex, confirming their similarity.

In this case, the best linear fit, calculated using orthogonal distance regression with the SCIPY.ODR[4] (hereafter ODR) considering the errors in both axes, between lithium abundances and stellar ages is

$$A(Li) = (-0.20 \pm 0.02)Age + (2.44 \pm 0.10). \quad (1)$$

[4]http://docs.scipy.org/doc/scipy/ reference/odr.html.

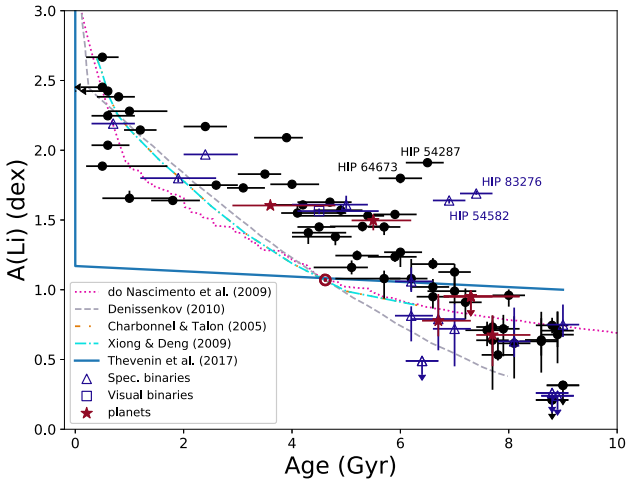

Figure 2. Connection between stellar ages and NLTE lithium abundances for our sample. The dark red filled stars indicate stars with detected planets, dark blue squares represent visual binaries, dark blue triangles show spectral binaries, and black filled circles represent single stars without planets detected. The models of Li depletion (referred in the text) were normalized to the solar Li abundance. In some cases, the lithium abundance errors are smaller than the points.

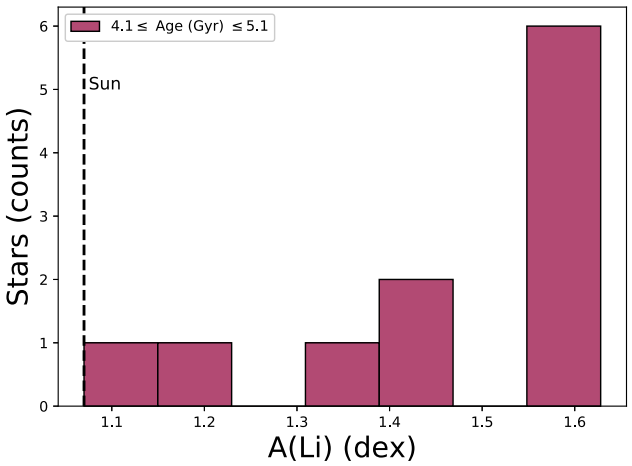

Figure 3. Distribution of A(Li) in a subsample of solar twins with ages between 4.1 and 5.1 Gyr. The NLTE Li abundance of the Sun is shown by the black dashed line. The gaps in the distribution stress the demand of observing more solar twins at this age interval.

We can notice in Fig. 5 how the Sun is Li-poor when compared to solar twins at the same age (see also the right-hand panel of Figs 1 and 3). The Sun is an outlier by $\sim 2\sigma$ from the Li–age correlation given in equation (1); furthermore, the Sun has the lowest Li abundance among solar twins of similar age (4.6 Gyr).

Using the equation (1) we found, for the whole sample, a correspondence between the lithium residuals (ΔA(Li)) and the stellar parameters, mass and [Fe/H]:

$$\Delta \mathrm{A(Li)} = -(3.55 \pm 1.11) + (3.47 \pm 1.09)\mathrm{M/M_{\odot}} - (1.17 \pm 0.52)[\mathrm{Fe/H}]. \quad (2)$$

This equation is in concordance with the models of Castro et al. (2009), who find that the lithium burning increases with increasing [Fe/H]; the opposite occurs for the other parameter where the lithium depletion is accentuated with decreasing in stellar mass. Furthermore, this result is compatible with the respective equation from Carlos et al. (2016) and have a more significant dependence in comparison with the one presented in this earlier work (3.2σ against 1.6σ for stellar mass and 2.3σ against 1.7σ for [Fe/H]).

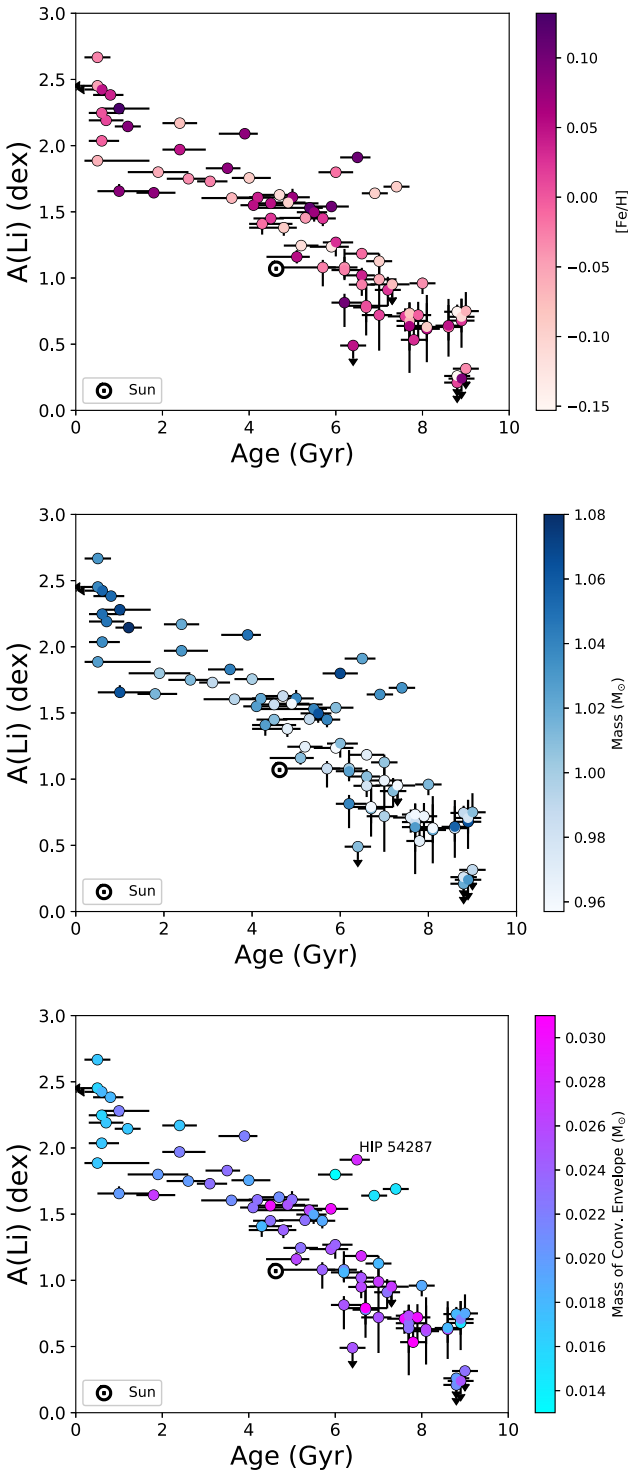

Figure 4. Lithium abundances versus stellar age colour coded by [Fe/H] (top panel), mass (middle panel), and the mass of the convective envelope (bottom panel). HIP 54287 is labelled in the lower panel because, as discussed in the text, it could have engulfed a planet.

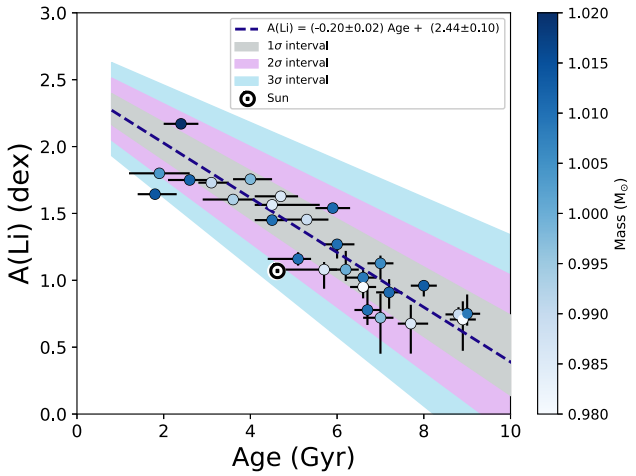

Figure 5. Lithium abundances versus stellar age as a function of mass in the interval $0.98 \leq M/M_{\odot} \leq 1.02$.

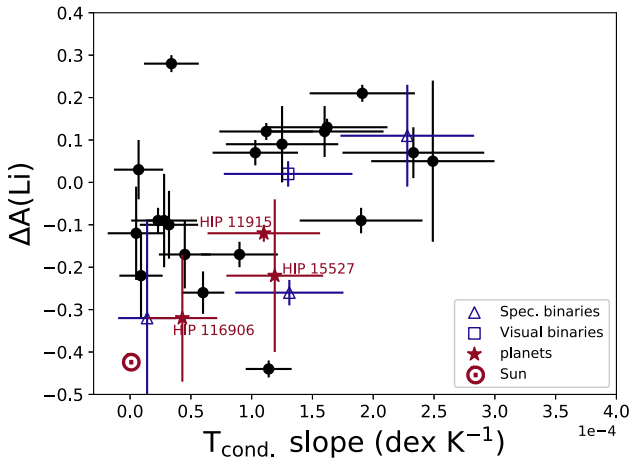

Figure 6. The lithium residuals (from Fig. 5) against the condensation temperature ($T_{cond.}$) slope from Bedell et al. (2018) for our subsample of stars with $0.98 \leq M/M_{\odot} \leq 1.02$. The name of the stars with detected planets are shown.

Fig. 6 shows ΔA(Li) for our subsample of stars with $0.98 \leq M/M_{\odot} \leq 1.02$ versus their respective condensation temperature slope corrected by the Galactic chemical evolution (T_c slope, third column of table 4 from Bedell et al. 2018).

The analysis of the condensation temperature trends can shed some light on the planetary formation scenarios since these T_c slopes are linked with the content of refractory elements ($T \gtrsim 900$ K, see discussion in Bedell et al. 2018) in stellar atmospheres, which can be associated to rocky planets (Meléndez et al. 2009).

The three stars with planets detected presented in Fig. 6 are: HIP 11915 that has a Jupiter twin detected with orbital period of 3830 ± 150 d and $m_p sini = 0.99 \pm 0.06\,M_{jup}$ (Bedell et al. 2015); HIP 116906 with one planet detected with orbital period of 572.38 ± 0.61 d and $m_p sini = 7.75 \pm 0.65\,M_{jup}$ (Butler et al. 2006); and HIP 15527 with one planet detected with orbital period of 595.86 ± 0.03 d and $m_p sini = 1.77 \pm 0.22\,M_{jup}$ (Jones et al. 2006).

We perform a Spearman correlation test considering the errors in both axes for the sample shown in Fig. 6 and found a Spearman rank coefficient $r_s = 0.47$ and a probability of 0.01 of our results arising by chance.

This tentative correlation indicates that the more lithium-depleted stars have less content of refractory material. According to Bedell et al. (2018), the Sun presents a refractory-to-volatile deficiency relative to 93 per cent of the sample of solar twins. If this depletion in refractory material is connected to the presence of planets or even the quantity of planets in our planetary system, what Fig. 6 shows is that the low lithium content of the Sun might be linked to the presence of rocky planets. Although we should be cautious as we do not have a complete census down to Earth masses of the planets hosted by other solar twins, the lower solar lithium content in comparison with stars at the same bin of age could be related to our Solar system configuration and possibly to terrestrial planets.

In addition, according to Tucci Maia et al. (2015) the Sun is also poor in Be. Despite the shallow trend of Be content with age for solar twins, Tucci Maia et al. (2015) showed that the solar Be is less abundant by $\sim$0.05 dex in comparison with other solar twins. This deficiency in Be might be linked to the Sun lower content of refractory material as well, as pointed out in Tucci Maia et al. (2015). Interestingly, the work of Botelho et al. (2019) found that the Sun has a lower [Th/Fe] ratio compared to solar twins at similar age, and also when corrected to its ZAMS (zero-age main sequence) value. This somewhat lower abundance of Th in the Sun is perhaps because Th is a highly refractory element (Lodders 2003), reflecting thus the refractory-depleted composition of the Sun, which could be linked to rocky planets (Meléndez et al. 2009).

5 CONCLUSIONS

We measured high-precision lithium abundances (median error of 0.036 dex) for a sample of 77 solar twins with high resolution and high signal-to-noise spectra from the HARPS spectrograph.

We confirm previous results showing the strong connection between lithium depletion and stellar ages and also identified a steeper Li depletion with stellar age for young solar twins (Age $\lesssim$2.0 Gyr).

Three of the four outliers in this work can be explained when considering the respective masses of their convective envelopes.

It seems that there is no significant difference in lithium depletion between known planet host stars and stars with no planets detected, when we analyse the lithium depletion and stellar age correlation. The same behaviour is found for visual and spectral binaries in comparison with single field stars.

We found that the Sun can be considered a lithium-poor star in comparison with other solar twins at similar age (by a factor of $\sim 2\sigma$). Also, our data suggest that stars with the lowest Li abundances are accompanied by a lower level of refractory elements. This could be explained by the presence of rocky planets and the unique architecture of the Solar system.

ACKNOWLEDGEMENTS

This study was financed in part by the Coordenação de Aperfeiçoamento de Pessoal de Nível Superior – Brasil (CAPES) – Finance Code 001. JM is thankful for the support of Fundação de Amparo à Pesquisa do Estado de São Paulo (FAPESP, 2014/18100-4, 2018/04055-8) and Conselho Nacional de Desenvolvimento Científico e Tecnológico (CNPq, Bolsa de Produtividade). LAdS acknowledges the financial support from the European Research Council (ERC) under the European Union's Horizon 2020 research

and innovation program (project FOUR ACES; grant agreement No. 724427).

Based on observations collected at the European Organisation for Astronomical Research in the Southern Hemisphere under ESO programs 188.C-0265, 183.D-0729, 292.C-5004, 097.C-0571, 092.C- 0721, 093.C-0409, 072.C-0488, 183.C-0972, 091.C-0936, 192.C- 0852, 196.C-1006, 076.C-0155, 096.C-0499, 185.D-0056, 192.C-0224, 075.C-0332, 090.C-0421, 091.C-0034, 077.C-0364, 089.C-0415, 60.A- 9036, 092.C-0832, 295.C-5035, 295.C-5031, 60.A-9700, 289.D-5015, 096.C-0210, 086.C-0284, 088.C-0323, 0100.D-0444, and 099.C-0491.

REFERENCES

Aguilera-Gómez C., Chanamé J., Pinsonneault M. H., Carlberg J. K., 2016, ApJ, 829, 127
Asplund M., Lambert D. L., Nissen P. E., Primas F., Smith V. V., 2006, ApJ, 644, 229
Asplund M., Grevesse N., Sauval A. J., Scott P., 2009, ARA&A, 47, 481
Ballot J., Brun A. S., Turck-Chièze S., 2007, ApJ, 669, 1190
Barnes S. A., 2007, ApJ, 669, 1167
Baumann P., Ramírez I., Meléndez J., Asplund M., Lind K., 2010, A&A, 519, A87
Beck P. G. et al., 2017, A&A, 602, A63
Bedell M., Meléndez J., Bean J. L., Ramírez I., Leite P., Asplund M., 2014, ApJ, 795, 23
Bedell M. et al., 2015, A&A, 581, A34
Bedell M. et al., 2018, ApJ, 865, 68
Bensby T., Lind K., 2018, A&A, 615, A151
Bonifacio P. et al., 2007, A&A, 462, 851
Botelho R. B. et al., 2019, MNRAS, 482, 1690
Brown B. P., Browning M. K., Brun A. S., Miesch M. S., Toomre J., 2008, ApJ, 689, 1354
Butler R. P. et al., 2006, ApJ, 646, 505
Carlos M., Nissen P. E., Meléndez J., 2016, A&A, 587, A100
Casey A. R. et al., 2016, MNRAS, 461, 3336
Casey A. R. et al., 2019, preprint (arXiv:1902.04102)
Castelli F., Kurucz R. L., 2003, in Piskunov N., Gray D. F., Weiss W. W., eds, New Grids of ATLAS9 Model Atmospheres. Modelling of Stellar Atmospheres, Vol. 210. AU Symposium Series, A20
Castro M., Vauclair S., Richard O., Santos N. C., 2009, A&A, 494, 663
Cescutti G., Molaro P., 2019, MNRAS, 482, 4372
Charbonnel C., Lagarde N., 2010, A&A, 522, A10
Charbonnel C., Talon S., 2005, Science, 309, 2189
Deepak Reddy B. E., 2019, MNRAS, 484, 2000
Delgado Mena E. et al., 2014, A&A, 562, A92
Denissenkov P. A., 2010, ApJ, 719, 28
Do Nascimento J. D., Jr., Castro M., Meléndez J., Bazot M., Théado S., Porto de Mello G. F., de Medeiros J. R., 2009, A&A, 501, 687
do Nascimento J.-D., Jr. et al., 2014, ApJ, 790, L23
dos Santos L. A. et al., 2016, A&A, 592, A156
dos Santos L. A. et al., 2017, MNRAS, 472, 3425
Fu X. et al., 2018, A&A, 610, A38
Gaia Collaboration, 2018, A&A, 616, A10
Gonzalez G., Carlson M. K., Tobin R. W., 2010, MNRAS, 403, 1368
Israelian G. et al., 2009, Nature, 462, 189
Jones H. R. A., Butler R. P., Tinney C. G., Marcy G. W., Carter B. D., Penny A. J., McCarthy C., Bailey J., 2006, MNRAS, 369, 249
Kim Y.-C., Demarque P., Yi S. K., Alexander D. R., 2002, ApJS, 143, 499
Lind K., Asplund M., Barklem P. S., 2009, A&A, 503, 541
Liu F., Asplund M., Yong D., Meléndez J., Ramírez I., Karakas A. I., Carlos M., Marino A. F., 2016, MNRAS, 463, 696
Lodders K., 2003, ApJ, 591, 1220
Lorenzo-Oliveira D. et al., 2018, A&A, 619, A73
Matsuno T., Aoki W., Beers T. C., Lee Y. S., Honda S., 2017, AJ, 154, 52
Mayor M. et al., 2003, The Messenger, 114, 20
Meléndez J., Asplund M., Gustafsson B., Yong D., 2009, ApJ, 704, L66
Meléndez J. et al., 2012, A&A, 543, A29
Meléndez J., Schirbel L., Monroe T. R., Yong D., Ramírez I., Asplund M., 2014, A&A, 567, L3
Meléndez J. et al., 2017, A&A, 597, A34
Monroe T. R. et al., 2013, ApJ, 774, L32
Montalbán J., Rebolo R., 2002, A&A, 386, 1039
Naef D. et al., 2010, A&A, 523, A15
Pace G., Pasquini L., 2004, A&A, 426, 1021
Pavlenko Y. V., Jenkins J. S., Ivanyuk O. M., Jones H. R. A., Kaminsky B. M., Lyubchik Y. P., Yakovina L. A., 2018, A&A, 611, A27
Ramírez I., Fish J. R., Lambert D. L., Allende Prieto C., 2012, ApJ, 756, 46
Ramírez I., Meléndez J., Asplund M., 2014, A&A, 561, A7
Ryan S. G., Norris J. E., Beers T. C., 1999, ApJ, 523, 654
Sandquist E. L., Dokter J. J., Lin D. N. C., Mardling R. A., 2002, ApJ, 572, 1012
Schirbel L. et al., 2015, A&A, 584, A116
Sneden C. A., 1973, PhD thesis, The University of Texas at Austin
Spada F., Demarque P., Kim Y.-C., Boyajian T. S., Brewer J. M., 2017, ApJ, 838, 161
Spina L. et al., 2018, MNRAS, 474, 2580
Spite F., Spite M., 1982, A&A, 115, 357
Takeda Y., Honda S., Kawanomoto S., Ando H., Sakurai T., 2010, A&A, 515, A93
Théado S., Vauclair S., 2012, ApJ, 744, 123
Thévenin F., Oreshina A. V., Baturin V. A., Gorshkov A. B., Morel P., Provost J., 2017, A&A, 598, A64
Tucci Maia M., Meléndez J., Castro M., Asplund M., Ramírez I., Monroe T. R., do Nascimento J. D., Jr., Yong D., 2015, A&A, 576, L10
Xiong D. R., Deng L., 2009, MNRAS, 395, 2013
Yan H.-L. et al., 2018, Nat. Astron., 2, 790
Yi S., Demarque P., Kim Y.-C., Lee Y.-W., Ree C. H., Lejeune T., Barnes S., 2001, ApJS, 136, 417
Zahn J.-P., 1994, A&A, 288, 829

This paper has been typeset from a TEX/LATEX file prepared by the author.